Rapid Communications

^{115}In NQR study with evidence for two magnetic quantum critical points in dual Ce site superconductor Ce_3PtIn_{11}

S. Kambe,[1] H. Sakai,[1] Y. Tokunaga,[1] R. E. Walstedt,[2] M. Kratochvílová,[3] K. Uhlířová,[3] and J. Custers[3]

[1]*Advanced Science Research Center, Japan Atomic Energy Agency, Tokai-mura, Ibaraki 319-1195, Japan*

[2]*Physics Department, The University of Michigan, Ann Arbor, Michigan 48109, USA*

[3]*Faculty of Mathematics and Physics, Charles University in Prague, Ke Karlovu 5, 121 16 Prague 2, Czech Republic*

(Received 18 October 2019; revised manuscript received 28 January 2020; accepted 29 January 2020; published 12 February 2020)

^{115}In nuclear quadrupole resonance (NQR) measurements have been carried out on Ce_3PtIn_{11}, a heavy fermion compound harboring two inequivalent Ce sites. This system exhibits magnetic transitions at $T_{1n} = 2.2$ K and $T_N = 2$ K, prior to entering a superconducting state below $T_c = 0.32$ K. Previous measurements imply that magnetism and superconductivity are spatially separated and only the Ce(2) sublattice orders magnetically, with a quantum critical point at pressure $p_c = 1.3$ GPa, while the Ce(1) sublattice is paramagnetic. However, the present nuclear relaxation rate behavior of $1/T_1 \propto \sqrt{T}$ reveals the presence of critical spin fluctuations indicative of close proximity to another quantum critical point, presumably at a small negative pressure, which is associated solely with the Ce(1) sublattice. The ordered wave vector is found to be most likely $(1/2, 1/2, h)$.

DOI: 10.1103/PhysRevB.101.081103

For materials in proximity of a "magnetic instability" or quantum critical point (QCP) where $T_N \to 0$, the abundance of low-lying and spatially extended antiferromagnetic (AFM) spin fluctuations of large amplitude are considered to be the cause for unconventional normal and superconducting (SC) states. Quite recently, a new heavy fermion (HF) antiferromagnet Ce_3PtIn_{11} was discovered. The material belongs to the $Ce_nT_mIn_{3n+2m}$ class of layered HF materials with most prominent representatives at ambient pressure being $CeIn_3$ [local moment (LM)-AFM; $T_N = 10.2$ K], $CeCoIn_5$ (HF-SC; $T_c = 2$ K), $CeRhIn_5$ (HF-AFM; $T_N = 3.8$ K), and Ce_2RhIn_8 (HF-AFM; $T_N = 2.8$ K). At ambient condition, Ce_3PtIn_{11} shows remarkable properties: Ce_3PtIn_{11} undergoes two successive magnetic transitions at $T_{1n} = 2.2$ K and $T_N = 2.0$ K, respectively, and becomes SC below $T_c = 0.35$ K [1]. Upon applying hydrostatic pressure T_{1n} and T_N reduce and intersect with the SC state at $p \approx 1.1$ GPa. Extrapolation of $T_N \to 0$ reveals a critical pressure of $p_c = 1.3$ GPa, which is considerable lower than in other compounds of this class, e. g., p_c of $CeRhIn_5$ yields ≈2.3 GPa [2,3]. Noteworthy, for $1.1 < p < 1.6$ GPa a non-Fermi-liquid state is observed which is characterized by an almost T-linear resistivity from T_c (≈0.7 K) to temperatures even higher than $T > 5$ K.

The discovery stirred a barely considered aspect; the majority of HF compounds investigated possess only one crystallographic independent LM site per unit cell. In HF compounds with multiple crystallographic inequivalent LM sites, such as Ce_3PtIn_{11}, the local environment of these two or more sites is different, leading to distinct different Kondo interaction strengths. It is easily conceivable that the ground state in such a compound is a microscopic coexistence of different electronic and magnetic sublattice states.

Figure 1 illustrates the unit cell of Ce_3PtIn_{11}. The Ce(1) surrounding is identical to Ce ions in Ce_2PtIn_8, which as a matter of fact is paramagnetic (PM) down to lowest temperatures [4]. The Ce(2) ion has a $CeIn_3$-like environment. On these bases it has been suggested that the Ce(1) sublattice is fully Kondo screened and makes the superconducting state while on the other hand the Ce(2) is responsible for the magnetic ordering [1]. As in Chevrel phases [5], borocarbides [6], and the high T_c's [7], magnetism and superconductivity hence would coexist as two spatial separated ground states in Ce_3PtIn_{11}, a novelty in HF compounds. The purpose of this ^{115}In NQR study is to find microscopic evidence for such a scenario.

Single-crystal samples of Ce_3PtIn_{11} were grown by the self-flux method. Details about the preparation and characterization of the sample have been reported previously [1]. NQR spectra under zero field on the ^{115}In nuclear spins ($I = 9/2$) were carried out using the standard $\pi/2$-π spin-echo method described in Ref. [8].

The crystal structure of Ce_3PtIn_{11} harbors 11 In ions per unit cell, which are situated at four inequivalent positions (see Fig. 1). Adhering to standard conventions, the most symmetric In(1) site has local tetragonal symmetry ($4/mmm$), followed by In(2) ($4mm$), In(3) ($2mm$), and In(4) ($2mm$). The corresponding zero-field NQR frequencies of the respective In sites can be derived using the Hamiltonian [9],

$$\mathscr{H}_{\rm NQR} = \frac{e^2qQ}{4I(2I-1)}\left[3I_z^2 - I(I+1) + \frac{1}{2}\eta(I_+^2 + I_-^2)\right], \quad (1)$$

where Q is the nuclear quadrupole moment ($^{115}Q = 0.810 \times 10^{-28}$ m^2 for ^{115}In), $eq = V_{zz}$ is the principal component of the electric field gradient tensor V_{ij}, and $\eta = (V_{xx} - V_{yy})/V_{zz}$ is the asymmetry parameter. The nuclear quadrupole resonance frequency is defined as $\nu_Q \equiv \frac{3e^2qQ}{2I(2I-1)h}$. In the absence of a magnetic field, each In site exhibits four frequencies labeled

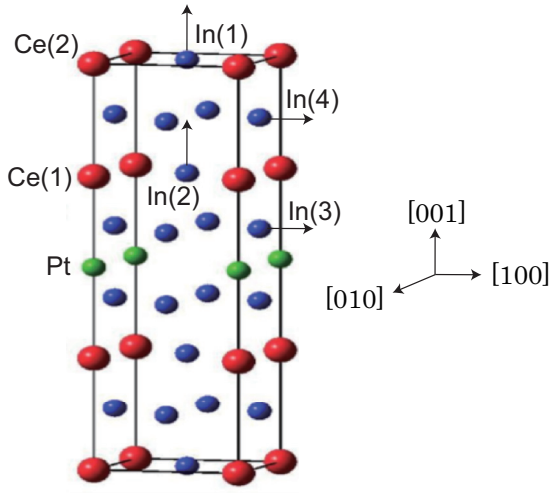

FIG. 1. Unit cell of Ce_3PtIn_{11} [space group $P4/mmm$ and $a = 4.6874(4)$ Å and $c = 16.8422(12)$ Å [4]]. Ce(1) and Ce(2) are considered to be PM and AFM ordered, respectively, below T_N [1]. The arrows indicate the direction of the quantization axis at each In site, i.e., V_{zz} determined by local symmetry and LDA calculations [10].

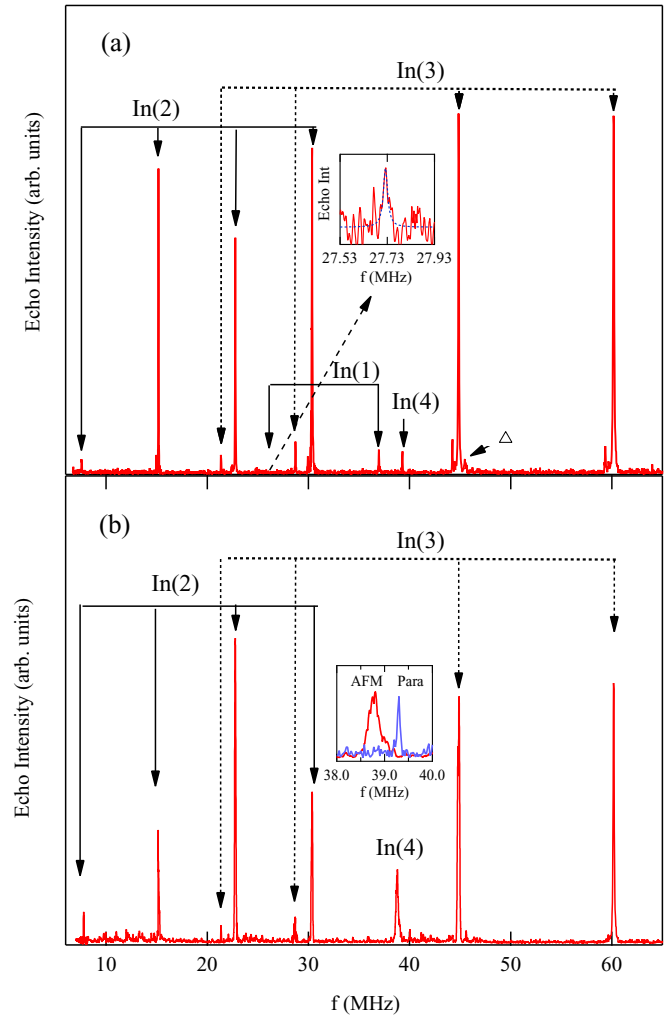

FIG. 2. (a) ^{115}In NQR spectra in the paramagnetic state (3.1 K) under zero field. Since the $f_3 = 3\nu_Q = 27.73$ MHz peak of the In(1) site is very weak (the intensity is ten times smaller than that of $f_4 = 4\nu_Q = 36.97$ MHz), it is presented separately as an inset. The △ peak is due to an impurity. (b) ^{115}In NQR spectra in the AFM ordered state (1.5 K) under zero field. The spectra of In(1) disappear and the spectrum of In(4) is broadened and shifted from 39.3 to 38.7 MHz. (Inset: The intensities are normalized, since they cannot be compared to each other precisely.) Although there seem to be some additional peaks (e.g., around 10 MHz), these were confirmed to be noise in longer acquisition time measurements.

by f_n ($n = 1$–4), being associated with the transitions between $|I_z = \pm 1/2\rangle$ and $|I_z = \pm 3/2\rangle$, $|I_z = \pm 3/2\rangle$ and $|I_z = \pm 5/2\rangle$, and so on. For the In(1) and In(2) sites $\eta = 0$, and f_n obeys the rule $f_n = n\nu_Q$. In contrast, the In(3) and In(4) have $\eta \neq 0$, hence the resonance frequencies do not follow such a simple relation.

In Fig. 2(a) we show the NQR spectrum in the paramagnetic state measured at a temperature of 3.1 K. The peaks are narrow, corresponding to only a small distribution of electric field gradients, as expected for a high-quality single-crystal sample. The signal intensity of In(1) and In(4) is weak compared with that of In(2) and In(3), since the spin-spin relaxation time T_2 is short at these sites (as well as the spin-lattice relaxation time T_1) (see Fig. 3).

Table I lists calculated values of $\nu_{Q,\mathrm{calc}}$ and η_{calc} for Ce_3PtIn_{11} derived from local density approximation (LDA) band calculations [10]. By comparing these calculated values with experimental ones from the present measurements, we were able to decompose the spectra. First, the In(2) site has $f_n(n = 1$–$4) = 7.58$, 15.16, 22.74, and 30.32 MHz, respectively, with $\eta = 0$. The experimentally determined ν_Q is smaller than the theoretical prediction ($\nu_{Q,\mathrm{calc}} = 9.6$ MHz). However, the implied shift in LDA calculations toward higher frequencies seems to be systematic for heavy atoms [10,11]. An effect of f-electron localization due to correlations is not included in the LDA calculations, however, such an effect on $\nu_{Q,\mathrm{calc}}$ is not significant [12], thus it is reasonable to use the $\nu_{Q,\mathrm{calc}}$ values for site assignment.

The f_n's for the In(3) site are easier to deduce. The transitions are located at 21.4, 28.7, 44.9, and 60.2 MHz in the spectra. As can be seen, f_3 and f_4 are accompanied by small satellite peaks at 44.3 and 59.4 MHz. They arise from the ^{113}In isotope ($I = 9/2$), which has a natural abundance of 4.3% (^{115}In is 95.7% abundant), and whose transitions obey the ratio $^{113}f_n/^{115}f_n = {}^{113}Q/{}^{115}Q$. The other low-intensity transition visible and marked by a △ in Fig. 2(a) has a very long T_1 (∼1 s). It may be from an unknown, nonmetallic phase outside of the sample. We derived ν_Q and η values for In(3) using the exact diagonalization of $\mathscr{H}_{\mathrm{NQR}}$ for the $I = 9/2$ case.

We identify the peak at 36.97 MHz as f_4 for the In(1) site for the following reasons. Accounting for $\eta = 0$ at the In(1) site, the f_1, f_2, and f_3 transitions should thus appear at 9.24, 18.48, and 27.73 MHz. Unfortunately, the first two were not detected owing to their short T_2 and small N (see Table I), while the f_3 peak at 27.73 Hz stands only marginally out of the background [see the inset in Fig. 2(a)].

The remaining unassigned peak at 39.3 MHz should therefore correspond to the In(4) site. The absence of a signal at $\frac{3}{4} \times 39.3 = 29.48$ MHz (if 39.3 MHz were $f_4 = 4\nu_Q$

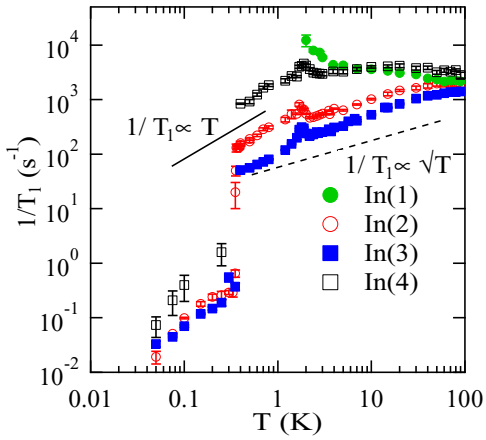

FIG. 3. T dependence of $1/T_1$ at the In(1–4) sites. There are no data for the In(1) site below T_N, since the signal disappears. Solid and dashed lines correspond to the Korringa ($1/T_1 \propto T$) and quantum critical AFM fluctuation ($1/T_1 \propto \sqrt{T}$) cases, respectively.

with $\eta = 0$) and $\frac{4}{3} \times 39.3 = 52.4$ MHz (if 39.3 MHz were $f_3 = 3\nu_Q$ with $\eta = 0$) in measurements employing a large acquisition time compels us to conclude that $\eta \neq 0$ for this site. However, we cannot state unambiguously whether the frequency corresponds to f_3 or f_4. Factoring in an expected small value of $\eta \sim 0.009$ causes the trend in frequency to shift between calculated and experimentally determined values (Table I); thus, the latter case most likely gives $\nu_Q \approx 9.8$ MHz.

To further understand the spectra, we note that each In site has a unique spin-lattice relaxation rate $1/T_1$ (Fig. 3). The foregoing assigned f_n peaks ($n = 1$–4) yielding the same T_1 are thus inherently linked to the same site.

Figure 2(b) displays the spectra in the AFM ordered state below T_N. The change of spectra at T_{1n} was too small to detected in the present measurement. Remarkably, the spectra of In(2) and In(3) remain very nearly unchanged. In the case of $CeIn_3$, upon entering the AFM state, a significant change is observed. Reflecting the appearance of internal fields, the f_1 spectrum splits and the other transitions shift to lower frequencies. In addition. these spectra become broader [13]. Similar results are reported for $CeRhIn_5$ [14], where the spectrum of the In(1) site separates into two resonances, while the spectrum of the In(2) takes a more complicated form owing to incommensurate helical magnetic ordering [15]. The change is more dramatic for Ce_2RhIn_8. Not only do the spectra of the In sites broaden for $T < T_N$, but the spectra nearly disappear [16]. The absence of such changes for Ce_3PtIn_{11} suggests that no internal field appears in the AFM ordered state at the In(2) and In(3) sites, which are located around the Ce(1) site in this system. We do observe a small shift and a clear broadening of the f_4 spectrum of the In(4) site around 39 MHz [see also the inset in Fig. 2(b)], confirming that this site is exposed to an internal field. Furthermore, the spectrum of the In(1) site vanishes, indicating that a large and/or distributed internal field appears at this particular site. We note that internal fields at In sites are induced through the transferred hyperfine coupling between the Ce $4f$ electron and the In nuclear spin, which is roughly proportional to $1/r^3$, where r is the distance between the Ce and In sites. These observations therefore strongly point to an ordered moment only at the Ce(2) site, corroborating the perception of a magnetic Ce(2) sublattice on the one hand, and coexisting on the other hand with a superconducting Ce(1) sublattice to be realized in Ce_3PtIn_{11}. This was pointed out in the Introduction, although the presence of a tiny moment at the Ce(1) site cannot be explicitly excluded from the data.

TABLE I. $\nu_{Q,\mathrm{calc}}$ and η_{calc} are calculated based on LDA band calculations [10]. ν_Q and η are obtained experimentally at 3.1 K. N is the number of atoms in the unit cell.

	$\nu_{Q,\mathrm{calc}}$ (MHz)	η_{calc}	ν_Q (MHz)	η	N
In(1)	11	0	9.24	0	1
In(2)	9.6	0	7.58	0	2
In(3)	17.3	0.077	15.1	0.237	4
In(4)	11.5	0.0089	∼9.8	≠0	4

In the following argument we make use of the fact that an internal field parallel to the quantization axis will have a much stronger effect on NQR frequencies than does a field perpendicular to the latter axis. Thus, the observed changes in NQR frequencies for In(1) and In(4) sites in the AFM state indicate that the internal field from AFM ordering has to lie parallel and perpendicular to the quantization axis for the In(1) and In(4) sites, respectively. Referring to Fig. 1, the internal field axis then lies along the [001] axis for In(1) and in the [100] plane at right angles to the quantization axis for In(4). We note two circumstances for the AFM propagation vector where these conditions would occur. First, if the magnetic wave vector is $\mathbf{q} = (0, 0, \frac{1}{2})$ with the ordered moment at the Ce(2) site $M_{\mathrm{or}} \parallel [001]$ axis, or second, an incommensurate case where $\mathbf{q} = (\frac{1}{2}, \frac{1}{2}, h)$, and where M_{or} has a large component along the [001] axis that is tilted to cause modulation of the hyperfine field. Noting that $\mathbf{q} = (\frac{1}{2}, \frac{1}{2}, \frac{1}{2})$ in $CeIn_3$ [17], $\mathbf{q} = (\frac{1}{2}, \frac{1}{2}, 0.297)$ under ambient pressure in $CeRhIn_5$ [18], $\mathbf{q} = (\frac{1}{2}, \frac{1}{2}, 0)$ in Ce_2RhIn_8 [19], and $\mathbf{q} = (\frac{1}{2}, \frac{1}{2}, \frac{1}{2})$ in $CePt_2In_7$ [20,21], the second possibility most likely holds for Ce_3PtIn_{11}. Neutron diffraction measurements are strongly motivated here for a more precise determination of the ordered AFM structure.

The NQR spectra in the SC state are almost identical with Fig. 2(b) (thus not shown), confirming that the internal fields resulting from magnetic ordering are still present below T_c. The latter results prove the coexistence of magnetism and superconductivity in Ce_3PtIn_{11}.

Further insights into the magnetic and superconducting properties were obtained by measuring T_1 as a function of temperature. A conventional inversion-recovery pulse technique was employed. Values of T_1 were obtained at the f_4 transition using fits to an appropriate relaxation function for spin $I = 9/2$ [$\eta = 0$ and 0.237 cases for In(1,2) and In(3) sites, respectively]. For the In(4) site we evaluated the data approximately using the relaxation function for $\eta = 0$.

Figure 3 displays the T dependence of $1/T_1$ at the In(1–4) sites. The AFM and SC transitions are clearly observed at the In(2,3,4) sites, confirming that antiferromagnetism and superconductivity coexist microscopically in Ce_3PtIn_{11}. The anomaly in $1/T_1$ at T_{1n} is quite small compared with that at

T_N. Above $T_N = 2$ K, the relaxation rate of In(2) and In(3) resembles the typical behavior of HF compounds [22,23]. At higher temperatures, $1/T_1$ is nearly temperature independent, indicating that the $4f$ electrons of Ce(1) ions are localized, in line with the observed Curie-Weiss behavior of the magnetization [1]. Upon lowering the temperature below $T^\star \sim 30$ K, $1/T_1$ decreases, signaling the crossover into a coherent Kondo regime. In this intermediate temperature range ($T_N < T < T^\star$) the relaxation rate varies nearly as $\sqrt{T}$.

In contrast, T_1 for the In(1) and In(4) sites shows a weak T dependence, reminiscent of the ^{115}In-T_1 behavior observed in the case of $4f$-localized $CeIn_3$ [13]. Upon lowering temperature, the In(1) site displays a rapid increase in $1/T_1$ at $T \sim 3$ K. Since the spin-lattice relaxation is induced by magnetic fluctuations perpendicular to the quantization axis, this enhancement gives evidence for the emergence of strong magnetic fluctuations in the Ce(2) basal plane. The temperature of this effect matches well with the maximum in the susceptibility, which has been attributed to the presence of two-dimensional (2D) short-range AFM correlations [1].

Below T_N, $1/T_1$ becomes nearly proportional to T, i.e., $1/T_1T$ is constant at the In(2,4) site, whereas the $1/T_1 \sim \sqrt{T}$ behavior persists at the In(3) site. The Korringa-type T dependence indicates that nonquantum critical heavy quasiparticles remain in the AFM ordered state above T_c, which is consistent with large C/T values at low temperature [1,24].

The entrance into the superconducting condensate is marked by a sudden drop of the spin relaxation rate at the In(2,3,4) sites, much as in $CePt_2In_7$ as well [25]. While the absence of a Hebel-Slichter coherence peak just below T_c already points to a non-s wave, unconventional type of superconducting state, the sharp decrease is rather unusual. Below T_c, $1/T_1$ does not follow the particular power-law behavior expected for a nodal gap state; rather, the jump implies a first-order-like transition. The physical origin of the sudden decrease of spin relaxation rate below T_c remains elusive [25]. The Korringa-type behavior reappears below 0.3 K. We do believe that this finite density of states is not due to impurities, but rather is indicative of a gapless nature for the low-lying excitation spectrum in the coexistence of SC and AFM states in analogy to $CeRhIn_5$ [26].

In the following, we discuss the implications of T_1 measurements above T_c. A $\sqrt{T}$ behavior has been found in the normal state of $CeRhIn_5$ [27], Ce_2RhIn_8 [15,16], Ce_2PdIn_8 [22], and, for instance, in the noncentrosymmetric HF superconductor $CeIrSi_3$ [28] when being tuned towards a QCP. It is associated with critical spin fluctuations as corroborated by the isotropic spin fluctuation model, which in such a case predicts the relation $1/T_1 \propto T\sqrt{\chi_q(T)} \propto \sqrt{T}$, where $\chi_q(T)$ represents the staggered susceptibility [29]. This observation thus strongly points to a close proximity to a QCP. The accompanying spin fluctuations are largely confined to the $Ce(1)_2PtIn_8$ layer (Fig. 1) as affirmed by the $1/T_1 \propto \sqrt{T}$ behavior of In(3). This site is encapsulated in the $Ce(1)_2PtIn_8$ layer and is farthest from the magnetic $Ce(2)In_3$ layer. The change of a $\sqrt{T}$ dependence to a Korringa-type behavior below T_N of $1/T_1$ for In(2) would therefore suggest that magnetic order suppresses these fluctuations.

The accumulated data are compatible with a scenario delineated in the Introduction: The Ce(2) ion located in the $CeIn_3$ layer maintains its $4f$-magnetic moment because of insufficient Kondo screening. The Ce(2) ions become magnetically coupled via a Ruderman-Kittel-Kasuya-Yosida (RKKY) interaction through the adjacent $Ce(1)_2PtIn_8$ layer establishing long-range AFM ordering at 2 K. The ordering persists in the superconducting state as inferred from the In(4) spectra. The previously reported QCP at $p_c = 1.3$ GPa thus is inherent to the Ce(2) sublattice [1]. In contrast, the Ce(1) ion is on the verge of magnetic ordering but the enhanced local on-site Kondo interaction just balances out the RKKY interaction. Thus the QCP of the $Ce(1)_2PtIn_8$ layer [Ce(1) sublattice] is located exactly at $p = 0$ or at slight negative pressure axis in the p-T phase diagram. Moreover, the close vicinity to a QCP strongly supports the view that $Ce(1)_2PtIn_8$ layer is primarily responsible for superconductivity.

Unlike recent experiments on hybrid heterostructures of $CeIn_3/CeCoIn_5$ and $CeRhIn_5/CeCoIn_5$ superlattices [30,31] where each block layer is several nm thick consisting of multiple unit cells of the respective material, Ce_3PtIn_{11} can be at best regarded as a stacking of perfectly matching monolayers or an infinite repetition of $CeIn_3/Ce_2PtIn_8$ interfaces. As such it is unlikely superconductivity would just be confined to the $Ce(1)_2PtIn_8$ layer, which is further supported by the rather isotropic behavior of H_{c2} [32], in contrast to results on $CeRhIn_5/CeCoIn_5$ superlattices [31]. However, the role of the $Ce(2)In_3$ layer in the SC properties is yet unclear. A spatial separation of superconductivity and magnetism could be linked to the two Ce sites, i.e., two different QCPs, which is an important issue to be addressed in future work on this system.

We are grateful for stimulating discussions with K. Ishida, Y. Kohori and H. Fukazawa. We thank H. Harima for showing us calculated ν_Q results. This work was supported by JSPS KAKENHI Grants No. 15H05884 (J-Physics), No. 15K05152, and No. 17K05522, and the REIMEI Research Program of JAEA. Research leading to these results was also conducted within the framework of the COST Action CA16218 (NANOCOHYBRI) of the European Cooperation in Science and Technology, the INTER-COST Project (No. LTC18024) of the Czech Ministry of Education, Youth and Sports, and the Grant Agency of the Czech Science Foundation (No. 19–23606S).

[1] J. Prokleška, M. Kratochvílová, K. Uhlířová, V. Sechovský, and J. Custers, Phys. Rev. B **92**, 161114(R) (2015).

[2] T. Park, F. Ronning, H. Q. Yuan, M. B. Salamon, R. Movshovich, J. L. Sarrao, and J. D. Thompson, Nature (London) **440**, 65 (2006).

[3] G. Knebel, D. Aoki, D. Braithwaite, B. Salce, and J. Flouquet, Phys. Rev. B **74**, 020501(R) (2006).

[4] M. Kratochvílová, M. Dusek, K. Uhlířová, A. Rudajevová, J. Prokleška, B. Vondráčková, J. Custers, and V. Sechovský, J. Cryst. Growth **397**, 47 (2014).

[5] Ø. Fisher, Appl. Phys. **16**, 1 (1978).
[6] L. C. Gupta, Adv. Phys. **55**, 691 (2006).
[7] I. Felner, U. Asaf, Y. Levi, and O. Millo, Phys. Rev. B **55**, R3374(R) (1997).
[8] H. Sakai, Y. Tokunaga, S. Kambe, H.-O. Lee, V. A. Sidorov, P. H. Tobash, F. Ronning, E. D. Bauer, and J. D. Thompson, Phys. Rev. B **83**, 140408(R) (2011).
[9] A. Abragam, *Principles of Nuclear Magnetism* (Clarendon, Oxford, UK, 1961).
[10] H. Harima, Physica B: Condens. Matter **378-380**, 246 (2006); (private communication).
[11] P. Blaha, K. Schwarz, and P. Herzig, Phys. Rev. Lett **54**, 1192 (1985).
[12] T. C. Kobayashi, K. Fijiwara, K. Takeda, H. Harima, Y. Ikeda, T. Adachi, Y. Ohishi, C. Geibel, and F. Steglich, J. Phys. Soc. Jpn. **82**, 114701 (2013).
[13] S. Kawasaki, M. Yashima, Y. Kitaoka, K. Takeda, K. Shimizu, Y. Oishi, M. Takata, T. C. Kobayashi, H. Harima, S. Araki, H. Shishido, R. Settai, and Y. Onuki, Phys. Rev. B **77**, 064508 (2008).
[14] N. J. Curro, P. C. Hammel, P. G. Pagliuso, J. L. Sarrao, J. D. Thompson, and Z. Fisk, Phys. Rev. B **62**, R6100(R) (2000).
[15] M. Yashima, S. Taniguchi, H. Miyazaki, H. Mukuda, Y. Kitaoka, H. Shishido, R. Settai, and Y. Onuki, Phys. Rev. B **80**, 184503 (2009).
[16] H. Fukazawa, T. Okazaki, K. Hirayama, Y. Kohori, G. Chen, S. Ohara, I. Sakamoto, and T. Matsumoto, J. Phys. Soc. Jpn. **76**, 124703 (2007).
[17] P. Morin, C. Vettier, J. Flouquet, M. Konczykowski, Y. Lassailly, J.-M. Mignot, and U. Welp, J. Low Temp. Phys. **70**, 377 (1988).
[18] W. Bao, P. G. Pagliuso, J. L. Sarrao, J. D. Thompson, Z. Fisk, J. W. Lynn, and R. W. Erwin, Phys. Rev. B **62**, R14621(R) (2000).
[19] W. Bao, P. G. Pagliuso, J. L. Sarrao, J. D. Thompson, Z. Fisk, and J. W. Lynn, Phys. Rev. B **64**, 020401(R) (2001).
[20] M. Raba, E. Ressouche, N. Qureshi, C. V. Colin, V. Nassif, S. Ota, Y. Hirose, R. Settai, P. Rodiére, and I. Sheikin, Phys. Rev. B **95**, 161102(R) (2017).
[21] N. Gauthier, D. Wermeille, N. Casati, H. Sakai, R. E. Baumbach, E. D. Bauer, and J. S. White, Phys. Rev. B **96**, 064414 (2017).
[22] H. Fukazawa, R. Nagashima, S. Shimatani, Y. Kohori, and D. Kaczorowski, Phys. Rev. B **86**, 094508 (2012).
[23] Y. Kohori, Y. Yamato, Y. Iwamoto, T. Kohara, E. D. Bauer, M. B. Maple, and J. L. Sarrao, Phys. Rev. B **64**, 134526 (2001).
[24] D. Das, D. Gnida, L. Bochenek, A. Rudenko, M. Daszkiewicz, and D. Kaczorowski, Sci. Rep. **8**, 16703 (2018).
[25] H. Sakai, Y. Tokunaga, S. Kambe, F. Ronning, E. D. Bauer, and J. D. Thompson, Phys. Rev. Lett. **112**, 206401 (2014).
[26] S. Kawasaki, T. Mito, Y. Kawasaki, G.-q. Zheng, Y. Kitaoka, D. Aoki, Y. Haga, and Y. Ōnuki, Phys. Rev. Lett. **91**, 137001 (2003).
[27] Y. Kohori, Y. Yamato, Y. Iwamoto, and T. Kohara, Eur. Phys. J. B **18**, 601 (2000).
[28] H. Mukuda, T. Fujii, T. Ohara, A. Harada, M. Yashima, Y. Kitaoka, Y. Okuda, R. Settai, and Y. Ōnuki, Phys. Rev. Lett. **100**, 107003 (2008).
[29] T. Moriya and K. Ueda, Adv. Phys. **49**, 555 (2000).
[30] M. Naritsuka, S. Nakamura, Y. Kasahara, T. Terashima, R. Peters, and Y. Matsuda, Phys. Rev. B **100**, 024507 (2019).
[31] M. Naritsuka, P. F. S. Rosa, Y. Luo, Y. Kasahara, Y. Tokiwa, T. Ishii, S. Miyake, T. Terashima, T. Shibauchi, F. Ronning, J. D. Thompson, and Y. Matsuda, Phys. Rev. Lett. **120**, 187002 (2018).
[32] M. Brando (private communication).